

# Partial-wave contributions to pairing in nuclei

Simone Baroni,<sup>1,2,\*</sup> Augusto O. Macchiavelli,<sup>3,†</sup> and Achim Schwenk<sup>2,4,5,‡</sup>

<sup>1</sup>*Institute for Nuclear Theory, University of Washington, Box 351550, Seattle, WA 98195, USA*

<sup>2</sup>*TRIUMF, 4004 Wesbrook Mall, Vancouver BC, V6T 2A3, Canada*

<sup>3</sup>*Nuclear Science Division, Lawrence Berkeley National Laboratory, Berkeley, CA 94720, USA*

<sup>4</sup>*ExtreMe Matter Institute EMMI, GSI Helmholtzzentrum für Schwerionenforschung GmbH, 64291 Darmstadt, Germany*

<sup>5</sup>*Institut für Kernphysik, Technische Universität Darmstadt, 64289 Darmstadt, Germany*

We present a detailed study of partial-wave contributions of nuclear forces to pairing in nuclei. For  $T = 1, J = 0$  pairing, partial waves beyond the standard  $^1S_0$  channel play an interesting role for the pair formation in nuclei. The additional contributions are dominated by the repulsive  $^3P_1$  partial wave. Their effects, and generally spin-triplet nuclear forces between paired nucleons, are influenced by the interplay of spin-orbit partners. We explore the impact of including partial waves beyond the  $^1S_0$  channel on neutron-neutron pairing gaps in semi-magic isotopic chains. In addition, we show that nuclear forces favor  $T = 1, J = 0$  over  $T = 0, J = 1$  pairing, except in low- $j$  orbitals. This is in contrast to the free-space motivation that suggests the formation of deuteron-like  $T = 0$  pairs in  $N = Z$  nuclei. The suppression of  $T = 0$  pairing is because the  $^3S_1$  strength is distributed on spin-orbit partners and because of the effects of the repulsive  $^1P_1$  channel and of D waves.

PACS numbers: 21.10.Dr, 21.60.Jz, 21.30.-x

## I. INTRODUCTION

Phenomenological energy density functionals are impressively successful in the description of medium-mass and heavy nuclei [1], but lack a microscopic connection to nuclear forces and seem to have reached the limits of improvement in the present functional form [2, 3]. This has led to exciting efforts, largely driven by effective field theory (EFT) ideas, to develop a universal energy density functional based on microscopic interactions [4, 5, 6, 7, 8]. These developments rely on the Hartree-Fock approximation as a good starting point for nuclei or on a perturbative expansion about nuclear matter. Both have become possible by evolving nuclear forces to low-momentum interactions using the renormalization group (RG) [9, 10, 11, 12, 13, 14].

In this paper, we follow Refs. [15, 16] and use existing energy density functionals in the particle-hole channel, to build a reasonable self-consistent single-particle basis, combined with low-momentum interactions  $V_{\text{low } k}$  [9, 10] in the pairing channel. The calculational details are given in Sect. II. This was shown to provide a good starting description of neutron-neutron and proton-proton pairing properties in semi-magic nuclei [15, 16, 17, 18]. In these and other [19, 20] calculations based on nuclear forces, the pairing interaction was restricted to the  $^1S_0$  partial wave. This is motivated by pairing in infinite matter (see, for example Ref. [21]), but in nuclei the paired nucleons are not in back-to-back-momentum configurations. Therefore, other partial waves can contribute to the pairing interaction for two particles with isospin  $T$

and total angular momentum  $J$ .

In Sect. III, we discuss partial-wave contributions to pairing interactions in nuclei. This is followed in Sect. IV by a detailed analysis of  $T = 1, J = 0$  pairing matrix elements in the  $sd$  and  $pf$  shells, where we focus on the effects of partial waves beyond the standard  $^1S_0$  channel. Spin-triplet partial-wave contributions to pairing in time-reversed states are found to depend on the spin-orbit configurations involved. In Sect. V, we explore the impact on  $T = 1$  pairing gaps in semi-magic isotopic chains. Our analysis of pairing matrix elements provides a simple explanation of the results observed in nuclei.

We extend the study of partial-wave contributions to  $T = 0$  pairing in Sect. VI, and compare the pairing strengths to the  $T = 1, J = 0$  channel at the level of low-momentum interactions. Since the deuteron is bound, the free-space motivation suggests the formation of  $T = 0, J = 1$  pairs in all  $N = Z$  nuclei [22]. In contrast, there is no direct observation of  $T = 0$  pairing to date. While we do not perform a calculation for nuclei, our analysis of  $T = 0, J = 1$  pairing matrix elements based on nuclear forces can provide a microscopic explanation for the suppression of  $T = 0$  pairing. For the  $^3S_1$  channel, the nuclear force strength is distributed on the spin-orbit partners, leading to a geometrical suppression in higher- $j$  orbitals. Moreover, the additional partial-wave contributions are dominated by the repulsive  $^1P_1$  channel with some smaller contributions due to D waves. As a result, in the absence of many-body effects on pairing, we find that low-momentum interactions favor  $T = 1, J = 0$  over  $T = 0, J = 1$  pairing, except in light  $N = Z$  nuclei where pairing is dominated by low- $j$  orbitals. The standard motivation for  $T = 0$  pairing in nuclei is therefore at best incomplete. We conclude and give an outlook in Sect. VII.

---

\*E-mail: baroni@phys.washington.edu

†E-mail: aomacchiavelli@lbl.gov

‡E-mail: schwenk@triumf.ca

## II. CALCULATIONAL DETAILS

The minimization of the energy density functional in the presence of pairing leads to solving the self-consistent Hartree-Fock-Bogoliubov (HFB) equations [1, 23] that determine the quasiparticle (q) basis,

$$\begin{pmatrix} h - \mu & \Delta \\ -\Delta^* & -(h - \mu) \end{pmatrix} \begin{pmatrix} U^q \\ V^q \end{pmatrix} = E_q \begin{pmatrix} U^q \\ V^q \end{pmatrix}. \quad (1)$$

Here  $h$  denotes the single-particle Hamiltonian,  $\mu$  the Fermi level,  $E_q$  is the quasiparticle energy and  $U^q, V^q$  the corresponding coefficients of the Bogoliubov transformation from single-particle to quasiparticle states. We use the Skyrme functional SLy4 [24] and first solve the Hartree-Fock (HF) equations,  $h\phi_a = \varepsilon_a^{\text{HF}}\phi_a$ , on a spherical mesh with 0.1 fm spacing and 16.0 fm box radius. Our results are stable with respect to increasing the radius and decreasing the mesh spacing. This defines the single-particle basis  $|a\rangle$ , using the shorthand label  $a \equiv n_a l_a j_a$  with radial quantum number  $n_a$ , orbital angular momentum  $l_a$  and total angular momentum  $j_a = l_a \pm 1/2$ .

Using the HF single-particle Hamiltonian, we then solve the HFB equations, where the state-dependent gap matrix  $\Delta$  for  $T = 1, J = 0$  pairing is given by

$$\Delta_{ab} = - \sum_{cd} \left( \sum_q U_c^q V_d^q \right) \sqrt{\frac{2j_c + 1}{2j_a + 1}} \frac{\sqrt{(1 + \delta_{ab})(1 + \delta_{cd})}}{2} \\ \times \langle ab | (1 - P_{12}) V_{\text{low } k} | cd \rangle_{J=0, T=1, T_z=-1}. \quad (2)$$

This defines the gap equation and we focus on neutron-neutron ( $T_z = -1$ ) pairing properties. The matrix elements of the pairing interaction in the second line of Eq. (2) are antisymmetrized using the exchange operator  $P_{12}$  and normalized, and  $\delta_{ab}$  is shorthand for  $\delta_{n_a n_b} \delta_{l_a l_b} \delta_{j_a j_b}$ . In general, after the HFB equations are solved self-consistently, one has to insert the resulting densities back into the single-particle Hamiltonian, which leads to a new set of single-particle states, in turn to a new HFB solution, and these iterations have to be repeated to obtain the fully self-consistent HFB solution. However, as shown in Sect. V, the feedback on the single-particle Hamiltonian can be neglected for pairing properties to a good approximation.

For the neutron-neutron pairing interaction, we start from the chiral N<sup>3</sup>LO two-nucleon (NN) potential ( $\Lambda = 500$  MeV) of Ref. [25] and use the RG to evolve this NN potential to low-momentum interactions  $V_{\text{low } k}$  with a smooth  $n_{\text{exp}} = 4$  regulator with  $\Lambda = 1.8 - 2.8 \text{ fm}^{-1}$  [10]. This evolution renders the many-body calculation more controlled [12, 13, 14] and provides a good starting point for connecting energy density functionals to nuclear forces [4, 18]. Based on the universality of  $V_{\text{low } k}$  [10, 13], we do not expect large differences starting from different N<sup>3</sup>LO potentials. As discussed in the following section, we calculate the  $jj$ -coupled pairing matrix elements entering the gap equation, Eq. (2), by expanding the HF single-particle states on the harmonic oscillator (HO)

basis. For pairing properties around the Fermi level, in particular for the lowest-quasiparticle-energy canonical state and average gaps presented in Sect. V, we have found that the HFB single-particle space can be restricted to states below 60 MeV (for hard potentials with large cutoffs, states up to  $\sim 1$  GeV are needed for convergence [19, 20]). Finally, an important direction for future work is to use energy density functionals in the particle-hole channel that are based on the same nuclear forces and to include many-body contributions to the pairing interaction. First results in this direction have been presented in Ref. [26].

In HFB theory, the interacting particles pair in orbitals related by time-reversal symmetry [27], where the radial quantum numbers can differ due to the Bogoliubov transformation [23]. Semiclassically, this is realized by two particles moving in the same orbit with opposite time order, so that  $(l_a, j_a) = (l_b, j_b)$  and  $(l_c, j_c) = (l_d, j_d)$  and hence the pairs have positive parity. For completeness, the gap equation is in the so-called phase convention II [27], for which the operation of the time-reversal operator  $\mathcal{T}$  on a single-particle state is given by  $\mathcal{T} |l_a j_a m_a\rangle = (-1)^{j_a - m_a} |l_a j_a - m_a\rangle$ , with magnetic quantum number  $m_a$ .

## III. PARTIAL-WAVE CONTRIBUTIONS TO PAIRING INTERACTIONS IN NUCLEI

The  $jj$ -coupled pairing matrix elements in the HF basis are obtained from the interaction matrix elements of  $V_{\text{low } k}$  in two-particle spherical HO states, which are calculated from the different partial-wave contributions using the standard recoupling formula,

$$\langle ab | (1 - P_{12}) V_{\text{low } k} | cd \rangle_{J, T, T_z} \Big|_{\text{HO basis}} \\ = \sum_{\substack{n, n', l, l', N, L \\ \lambda, \lambda', S, J_{\text{rel}}}} \frac{\widehat{j}_a \widehat{j}_b \widehat{j}_c \widehat{j}_d \widehat{\lambda}^2 \widehat{\lambda}'^2 \widehat{S}^2 \widehat{J}_{\text{rel}}^2}{\sqrt{(1 + \delta_{ab})(1 + \delta_{cd})}} \left\{ \begin{matrix} L & l & \lambda \\ S & J & J_{\text{rel}} \end{matrix} \right\} \\ \times \left\{ \begin{matrix} L & l' & \lambda' \\ S & J & J_{\text{rel}} \end{matrix} \right\} \left\{ \begin{matrix} l_a & 1/2 & j_a \\ l_b & 1/2 & j_b \\ \lambda & S & J \end{matrix} \right\} \left\{ \begin{matrix} l_c & 1/2 & j_c \\ l_d & 1/2 & j_d \\ \lambda' & S & J \end{matrix} \right\} \\ \times \langle nlNL | n_a l_a n_b l_b \lambda \rangle \langle n' l' N L | n_c l_c n_d l_d \lambda' \rangle (-1)^{\lambda + \lambda'} \\ \times (1 - (-1)^{l + S + T}) \langle nl | V_{\text{low } k}^{T, T_z} | n' l' S J_{\text{rel}} \rangle. \quad (3)$$

Here we use  $\widehat{x} = \sqrt{2x + 1}$  and standard notation for  $6j$  and  $9j$  symbols [28]. The bracket  $\langle nlNL | n_a l_a n_b l_b \lambda \rangle$  denotes Talmi-Moshinsky brackets [29], with relative and center-of-mass radial and orbital quantum numbers  $n, l, N, L$ , and total orbital angular momentum of the pair  $\lambda$ . The two-body spin is given by  $S$  and  $\mathbf{J}_{\text{rel}} = \mathbf{l} + \mathbf{S}$  denotes the relative total angular momentum. We use the standard notation  $2^{S+1} l_{J_{\text{rel}}}$  to denote the different partial

waves, which we list for completeness:

$$\text{for } T = 1: \quad {}^1S_0 \quad {}^3P_{0,1,2} \quad {}^1D_2 \quad {}^3F_{2,3,4} \quad {}^1G_4 \quad \dots$$

$$\text{for } T = 0: \quad {}^3S_1 \quad {}^1P_1 \quad {}^3D_{1,2,3} \quad {}^1F_3 \quad {}^3G_{3,4,5} \quad \dots$$

Additional restrictions come into play in the pairing problem when the total angular momentum of the paired nucleons is  $J = 0$ . Because  $\mathbf{L} + \mathbf{J}_{\text{rel}} = \mathbf{J}$ , one therefore has  $L = J_{\text{rel}}$  for  $J = 0$ . Moreover, because the parity of the pair is positive, it follows that the relative and center-of-mass orbital angular momentum  $l$  and  $L$  must have the same parity. As a result, the relative orbital and total angular momentum  $l$  and  $J_{\text{rel}}$  also have the same parity, and therefore only uncoupled channels  ${}^{2S+1}l_{J_{\text{rel}}=l}$  contribute to  $T = 1, J = 0$  pairing matrix elements. On the other hand,  $T = 0, J = 1$  matrix elements are not affected by these additional constraints and coupled channels also contribute to the pair formation in nuclei.

In summary, this shows that the  ${}^1S_0$  and  ${}^3S_1 - {}^3D_1$  partial waves are not the only channels contributing to  $T = 1$  and  $T = 0$  pairing in nuclei. In addition, the following partial waves are part of the pairing interaction:

$$T = 1, J = 0: \quad {}^1S_0 \quad {}^3P_1 \quad {}^1D_2 \quad {}^3F_3 \quad {}^1G_4 \quad \dots$$

$$T = 0, J = 1: \quad {}^3S_1 \quad {}^1P_1 \quad {}^3D_{1,2,3} \quad {}^1F_3 \quad {}^3G_{3,4,5} \quad \dots$$

Interestingly, both  ${}^3P_1$  and  ${}^1P_1$  partial waves are repulsive at the relevant energies [30]. We therefore expect a reduction of the pairing gap compared to studies based on the standard S-wave interactions.

#### IV. $T = 1, J = 0$ PAIRING MATRIX ELEMENTS

The  $sd$  and  $pf$  shells are very useful for understanding the results observed in nuclei in Sect. V. These two major shells are small enough to allow a simple study and at the same time they are complex enough to draw general conclusions. In Figs. 1 and 2, we show the  $jj$ -coupled  $T = 1, J = 0$  pairing matrix elements in the  $sd$  and  $pf$  shells based on the smooth  $V_{\text{low } k}$  evolved from the  $N^3\text{LO}$  potential of Ref. [25] to  $\Lambda = 2.0 \text{ fm}^{-1}$ . Here, we give neutron-proton ( $T_z = 0$ ) matrix elements in order to compare to the  $T = 0, J = 1$  pairing strengths in Sect. VI. The contributions from isospin-dependent nuclear forces that distinguish between the  $T = 1, T_z = 0$  and  $T = 1, T_z = -1$  channel (used in the calculations for nuclei) are small and do not change this analysis. The matrix elements are in the HO basis with  $\hbar\omega = 10 \text{ MeV}$ , but the general effects of partial waves are qualitatively similar for other values of  $\hbar\omega$  or in the HF basis.

As expected based on NN phase shifts, the pairing matrix elements are attractive for the  ${}^1S_0$  channel. In addition, we find that the attractive  ${}^1S_0$  contribution increases approximately linearly with increasing  $j_a$  or  $j_b$  within each  $(l_a, l_b)$  group. This can be understood using a semiclassical picture. In the classical limit, the plane

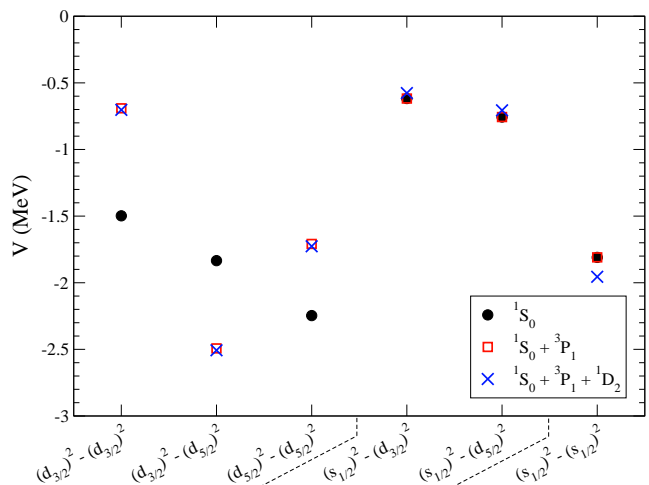


FIG. 1:  $T = 1, J = 0$  pairing matrix elements in the  $sd$  shell. Results are shown for the RG-evolved  $N^3\text{LO}$  potential of Ref. [25] with  $\Lambda = 2.0 \text{ fm}^{-1}$ , represented in two-particle HO states with  $\hbar\omega = 10 \text{ MeV}$ . The label  $(l_a j_a)^2 - (l_b j_b)^2$  denotes the bra–ket quantum numbers and we have grouped matrix elements according to  $(l_a, l_b)$ . In the  $sd$  shell, the two-particle quantum numbers combined with  $J = 0$  restrict the summation over partial waves to  $l \leq 2$ .

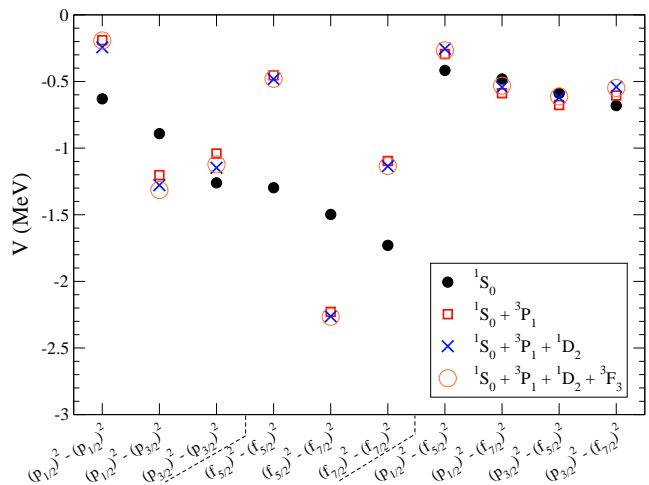


FIG. 2: Same as Fig. 1 but for the  $pf$  shell, where partial waves with  $l \leq 3$  can contribute to  $T = 1, J = 0$  pairing matrix elements.

of motion of a particle is determined by the orbital angular momentum vector  $\ell$ . Therefore, two particles moving in time-reversed orbits with total angular momentum zero will have opposite angular momentum vectors. The larger the value of  $l_a, l_b$ , the closer the situation will be to the classical picture and the more aligned the orbital angular momentum vectors will be (see also Ref. [31, Sect. 2.2]). Hence, the overlap between the orbitals is larger with increasing orbital angular momentum. The same holds with increasing total angular momentum and

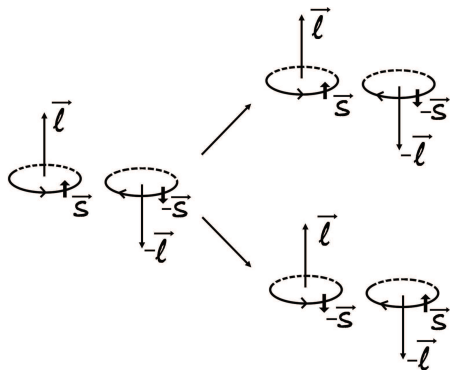


FIG. 3: Illustration of two particles in time-reversed states with  $j_> = l + 1/2$  (left) scattering to the same  $(j_>)^2$  configuration (top right) or to the  $(j_<)^2$  configuration involving the spin-orbit partner  $j_< = l - 1/2$  (bottom right).

the larger overlap leads to the more attractive  $^1S_0$  contribution for larger  $j_a$  or  $j_b$  within each  $(l_a, l_b)$  group.

### A. Spin-triplet contributions

The  $^3P_1$  partial wave is repulsive at the relevant energies [30]. However, the contributions to the pairing matrix elements in Figs. 1 and 2 are clearly more complicated. While the  $^3P_1$  contribution is repulsive between the same spin-orbit partners  $(j_>)^2 - (j_>)^2$  and  $(j_<)^2 - (j_<)^2$  (as expected from phase shifts), we find an attractive contribution to the pairing matrix elements connecting  $(j_>)^2 - (j_<)^2$  and  $(j_<)^2 - (j_>)^2$  configurations, where the spin-orbit partners are denoted by  $j_> = l + 1/2$  and  $j_< = l - 1/2$ . This effect can be seen prominently in the  $pf$  shell in Fig. 2. This is a general property of spin-triplet nuclear forces and applies also to  $T = 0, J = 1$  pairing matrix elements.

The different configurations for scattering of two particles in time-reversed states are illustrated in Fig. 3. In the semiclassical picture, the spin  $\mathbf{s}$  of the particle will be in the direction or opposite to the orbital angular momentum vector  $\boldsymbol{\ell}$  for the  $j_>$  or  $j_<$  configuration, respectively. If the two particles scatter from the  $j_>$  orbital to its spin-orbit partner  $j_<$  (left to bottom right in Fig. 3), they will experience a spin flip that would not occur in the case that the particles remain in the same  $j_>$  orbital (left to top right in Fig. 3). This spin flip leads to a relative sign in the spin part of the wave function  $|\uparrow\mathcal{T}(\uparrow)\rangle = |\uparrow\downarrow\rangle = (|S = 1\rangle + |S = 0\rangle)/\sqrt{2}$  (for the left configuration in Fig. 3) versus  $|\downarrow\mathcal{T}(\downarrow)\rangle = -|\downarrow\uparrow\rangle = (-|S = 1\rangle + |S = 0\rangle)/\sqrt{2}$  (for the bottom right configuration), which results in the relative sign difference of spin-triplet partial wave contributions to  $(j_>)^2 - (j_<)^2$  and  $(j_<)^2 - (j_>)^2$  versus  $(j_>)^2 - (j_>)^2$  and  $(j_<)^2 - (j_<)^2$  configurations. This also holds for  $(l_a j_a)^2 - (l_b j_b)^2$  matrix elements with  $l_a \neq l_b$ , leading to an additional sign for gen-

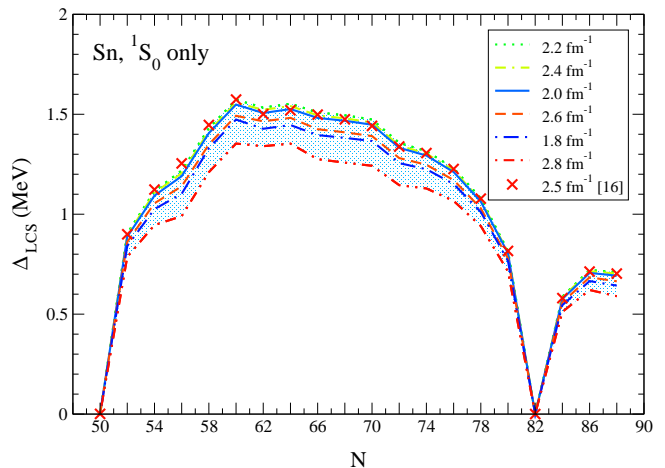


FIG. 4: Cutoff dependence of the LCS gaps in the tin isotopes including only the  $^1S_0$  contribution to the pairing interaction. The order in the legend corresponds to the order of the curves. The crosses denote the results of Ref. [16], based on a smooth  $V_{\text{low } k}$  evolved from the Argonne  $v_{18}$  potential to  $\Lambda = 2.5 \text{ fm}^{-1}$  with  $n_{\text{exp}} = 6$ .

eral upper-lower spin-orbit configurations  $(j_{a>})^2 - (j_{b<})^2$  and  $(j_{a<})^2 - (j_{b>})^2$ .

### V. $T = 1$ PAIRING GAPS

As measures of  $T = 1$  pairing in nuclei, we calculate both the lowest-quasiparticle-energy canonical state (LCS) gap and an average gap. The former is defined as the diagonal pairing gap  $\Delta_{aa}$  of Eq. (2), where the LCS state  $a$  is the canonical state with the lowest quasiparticle energy  $E_a$  given by

$$E_a = \sqrt{(\varepsilon_a - \mu)^2 + \Delta_{aa}^2}. \quad (4)$$

The canonical basis is defined by diagonalizing the density matrix, and  $\varepsilon_a$  is the canonical single-particle energy. The LCS state is close to the Fermi level using the definition of Eq. (4). We introduce the average gap as

$$\bar{\Delta} = \frac{\sum_a \left( \sum_q U_a^q V_a^q \right) (2j_a + 1) \Delta_{aa}}{\sum_a \left( \sum_q U_a^q V_a^q \right) (2j_a + 1)}. \quad (5)$$

The factor  $(\sum_q U_a^q V_a^q) (2j_a + 1)$  weighs states according to the degeneracy of the level and averages over an energy window around the Fermi level, which is approximately given by one shell above and below the Fermi level (for example,  $\approx \mu \pm 10 \text{ MeV}$  in  $^{120}\text{Sn}$ ).

We compare the theoretical LCS and average gaps calculated for even-even nuclei to experimental gaps based on the three-point mass formula centered on odd nuclei

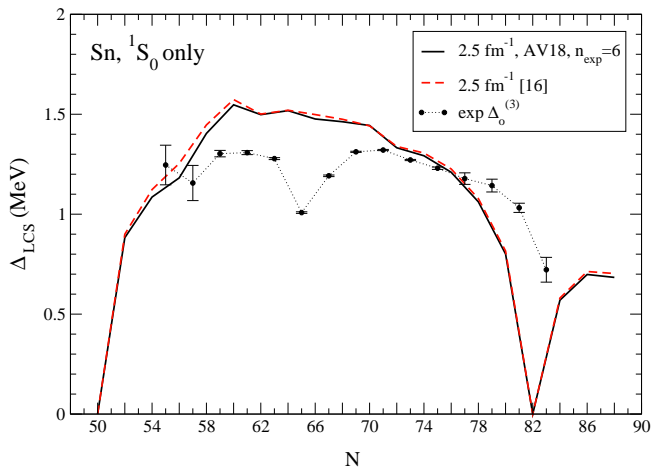


FIG. 5: Comparison of the LCS gaps in the tin isotopes obtained using a smooth  $V_{\text{low } k}$  evolved from the Argonne  $v_{18}$  potential to  $\Lambda = 2.5 \text{ fm}^{-1}$  with  $n_{\text{exp}} = 6$  and those of Ref. [16] using the same pairing interaction. Experimental gaps based on the three-point mass formula are shown for comparison.

(odd  $N$ ) [32, 33],

$$\Delta_o^3(N) = \frac{(-1)^N}{2} [B(N+1, Z) - 2B(N, Z) + B(N-1, Z)], \quad (6)$$

using experimental binding energies  $B(N, Z)$  of Ref. [34].

For low-momentum interactions, superfluid properties are dominated by states around the Fermi level and the contributions from the right-hand side of the gap equation, Eq. (2), fall off as particle pairs scatter to higher-lying states [18]. Therefore, our results are independent of the HO basis parameters, as long as the HF states around the Fermi level are reproduced. We have found that 10 oscillator shells are sufficient for  $6 < \hbar\omega < 18 \text{ MeV}$ . The dependence of the pairing gaps on the HO basis parameters is at the keV level over this range.

We first study the cutoff dependence of the LCS gaps in Fig. 4. For simplicity, we here include only the  $^1S_0$  contribution. We find that the cutoff variation is small overall and for  $2.0 \text{ fm}^{-1} \lesssim \Lambda \lesssim 2.5 \text{ fm}^{-1}$  the gaps are approximately cutoff independent. Next, we check our results against the gaps obtained in Ref. [16] using the same pairing interaction: the  $^1S_0$  part of the smooth  $V_{\text{low } k}$  evolved from the Argonne  $v_{18}$  potential to  $\Lambda = 2.5 \text{ fm}^{-1}$  with  $n_{\text{exp}} = 6$  (and the same Skyrme functional SLy4 in the particle-hole channel). The very good agreement is shown in Fig. 5. The gaps are within 0.5% for almost all tin isotopes, with a couple of them ( $N = 54$  and  $56$ ) showing a larger (but still small) difference of 3%. This demonstrates that the truncation after the first HFB iteration introduces a negligible error for pairing gaps. In the following, all results are based on the RG-evolved  $N^3\text{LO}$  potential of Ref. [25] with  $\Lambda = 2.0 \text{ fm}^{-1}$  and  $n_{\text{exp}} = 4$ .

In Fig. 6, we plot the state dependence of the canonical pairing gap  $\Delta_{aa}$  versus the canonical single-particle en-

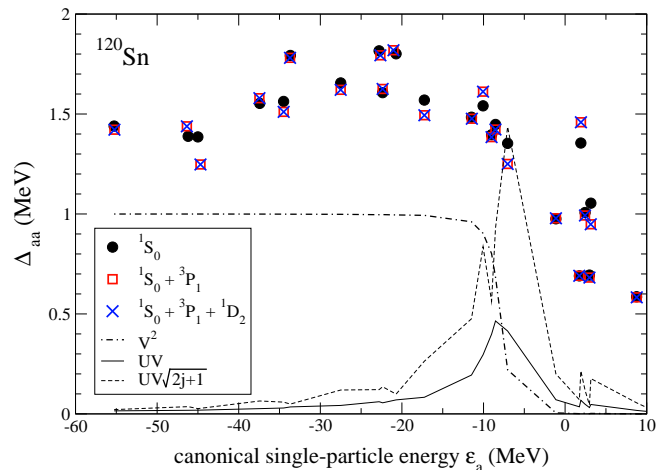


FIG. 6: State-dependent canonical pairing gap  $\Delta_{aa}$  in  $^{120}\text{Sn}$  versus canonical single-particle energy  $\varepsilon_a$ . In addition, we show the occupation factor  $\sum_q V_a^q V_a^q$  (labeled  $V^2$ ), the  $\sum_q U_a^q V_a^q$  factor (labeled  $UV$ ), and the  $(\sum_q U_a^q V_a^q) \sqrt{2j_a + 1}$  factor (labeled  $UV\sqrt{2j+1}$ ) that enters the gap equation, Eq. (2). The  $y$ -axis for the different factors is dimensionless and the factors corresponding to the three partial-wave cases are the same on this scale.

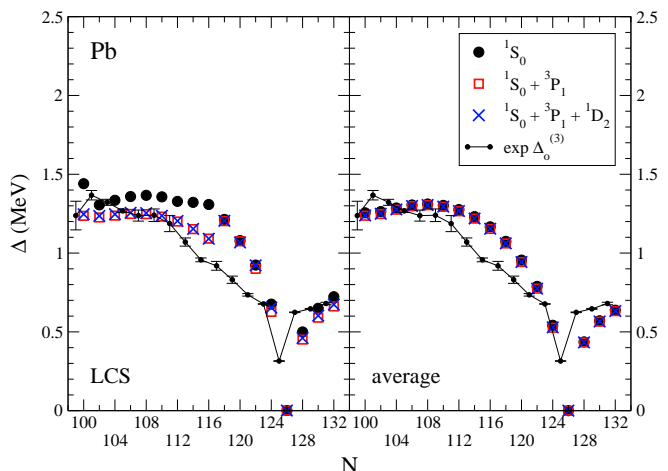


FIG. 7: LCS and average gaps in the lead isotopes with increasing partial-wave contributions to the pairing interaction. Experimental gaps based on the three-point mass formula are shown for comparison.

ergy  $\varepsilon_a$ . The occupation factor ( $V^2$ ) and the  $UV$  factors are included to show the Fermi level. As expected from the pairing matrix elements, we observe that the impact of the  $^3P_1$  partial wave is attractive for some states (pairing gap is increased) and repulsive for others (pairing gap is decreased). This is due to the interplay between upper-lower spin-orbit configurations for spin-triplet contributions to pairing, discussed in Sect. IV A. Given the  $(\sum_q U_a^q V_a^q) \sqrt{2j_a + 1}$  factor shown in Fig. 6, the effect of

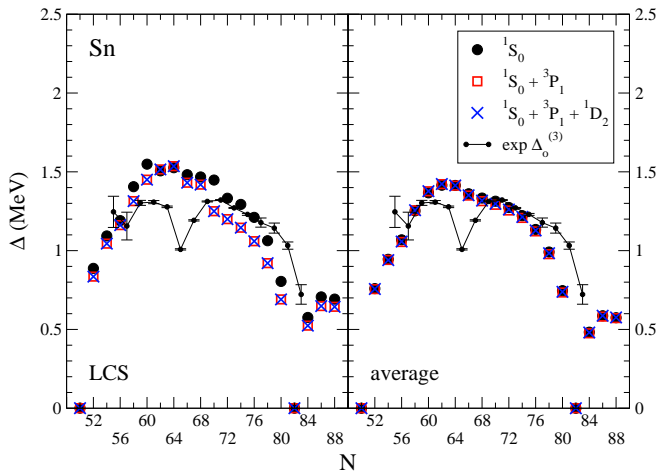


FIG. 8: Same as Fig. 7, but for tin isotopes.

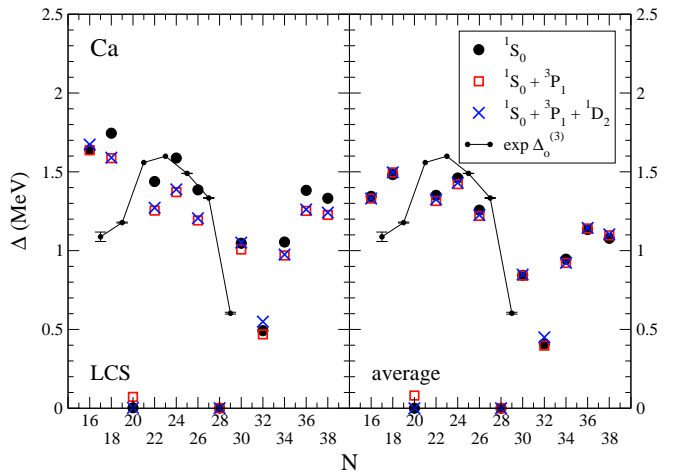


FIG. 10: Same as Fig. 7, but for calcium isotopes.

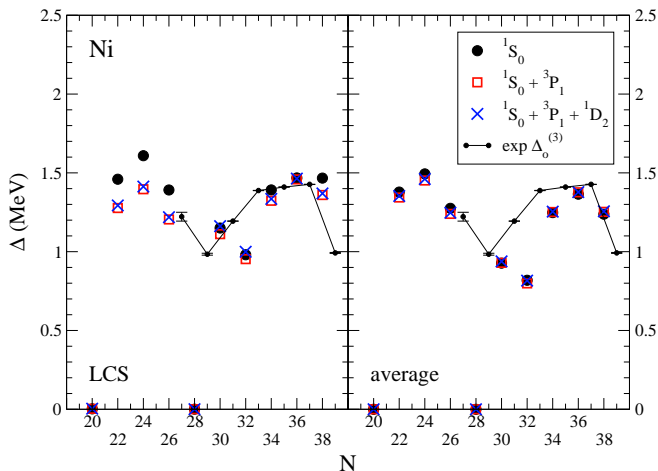


FIG. 9: Same as Fig. 7, but for nickel isotopes.

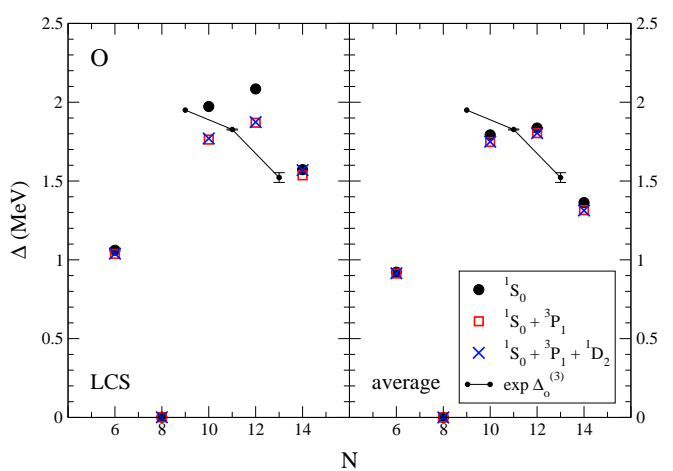


FIG. 11: Same as Fig. 7, but for oxygen isotopes.

the  $^3P_1$  partial wave on  $\Delta_{aa}$  in the gap equation, Eq. (2), is driven by the sign of the  $^3P_1$  contribution to the pairing matrix elements  $\langle aa | (1 - P_{12}) V_{\text{low } k} | ff \rangle_{J=0, T=1, T_z=-1}$ , where  $f$  denotes the LCS state close to the Fermi level where  $(\sum_q U_a^q V_a^q) \sqrt{2j_a + 1}$  is peaked. Following the analysis of Sect. IV A, for the LCS state ( $a = f$ ) or if  $a$  and  $f$  are the same upper or lower spin-orbit configurations, the  $^3P_1$  partial wave will decrease the state-dependent pairing gap  $\Delta_{aa}$ , while for different spin-orbit states  $a$ , the  $^3P_1$  contribution will increase  $\Delta_{aa}$ . Moreover, as expected from Figs. 1 and 2, the impact of higher partial waves beyond the  $^3P_1$  channel is small in Fig. 6 and for  $T = 1$  pairing gaps in other nuclei.

We present a more global study of neutron-neutron pairing gaps by calculating the LCS and average gaps for even-even nuclei in the lead, tin, nickel, calcium and oxygen isotopes in Figs. 7-11. The theoretical gaps are shown with increasing partial-wave contributions to the pairing interaction and in comparison to the experimental gaps

based on the three-point mass formula, Eq. (6), centered on the neighboring odd nuclei. Higher partial waves were also included in Ref. [26]. The additional contributions beyond the standard  $^1S_0$  channel are dominated by the  $^3P_1$  partial wave. They lead to a decrease of the LCS gaps of up to 15% and can change the isotopic dependence at this level. On the other hand, because of the interplay of spin-orbit configurations for the spin-triplet  $^3P_1$  channel and the resulting alternation of repulsive and attractive contributions to the state-dependent pairing gap in Fig. 6, we find that the average gap changes little when additional partial waves beyond the  $^1S_0$  channel are included. This shows that the impact of the  $^3P_1$  contribution depends on the definition of theoretical gap. We therefore conclude that future studies should compare directly calculated odd-even mass differences to the experimental gaps. This has recently been carried out in Ref. [17] using only the  $^1S_0$  contribution to the pairing interaction.



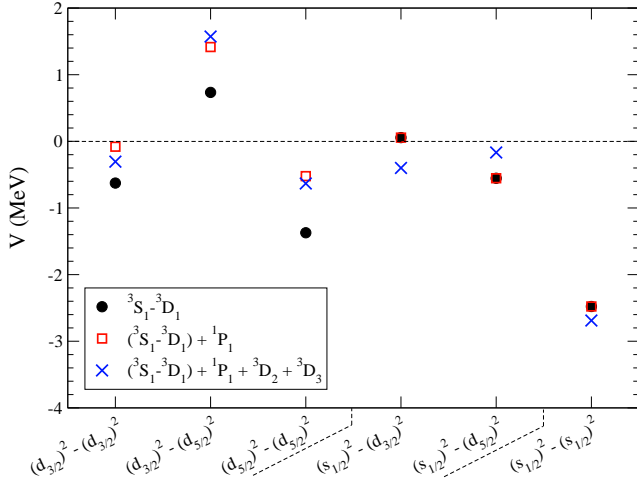


FIG. 12:  $T = 0, J = 1$  pairing matrix elements in the  $sd$  shell based on the same RG-evolved  $N^3\text{LO}$  potential as used to calculate the  $T = 1, J = 0$  pairing matrix elements in Fig. 1.

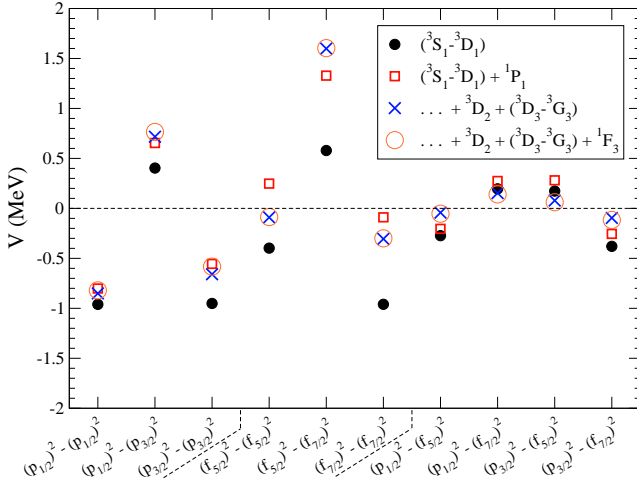


FIG. 13: Same as Fig. 12 but for the  $pf$  shell, where partial waves up to the  $^3G_3$  channel can contribute to  $T = 0, J = 1$  pairing matrix elements.

## VI. $T = 0, J = 1$ PAIRING MATRIX ELEMENTS

We turn to the case of neutron-proton  $T = 0, J = 1$  pairing, with a focus on the relative pairing strengths compared to the  $T = 1, J = 0$  channel. In Figs. 12 and 13, we show the  $jj$ -coupled  $T = 0, J = 1$  pairing matrix elements in the  $sd$  and  $pf$  shell. The matrix elements are in the HO basis with  $\hbar\omega = 10$  MeV, but the general effects of partial waves are qualitatively similar for other values of  $\hbar\omega$  or in the HF basis. While all  $T = 1, J = 0$  pairing matrix elements are attractive at the S-wave level, for  $T = 0$  pairing the S-wave contribution is given by the spin-triplet  $^3S_1 - ^3D_1$  channel, which is influenced by the interplay between spin-orbit configurations

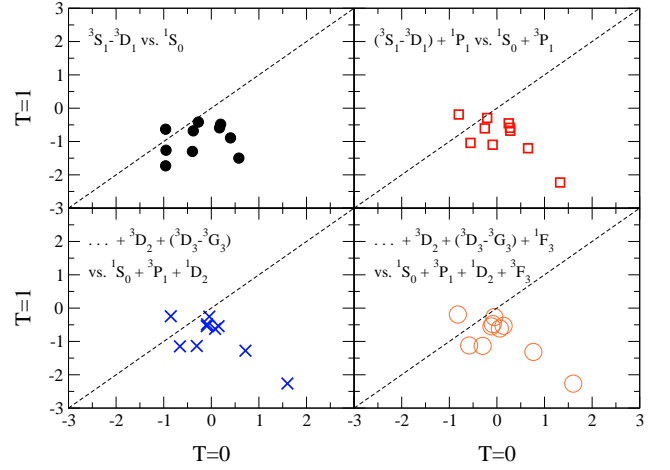


FIG. 14: Comparison of  $T = 1, J = 0$  versus  $T = 0, J = 1$  pairing matrix elements in the  $pf$  shell. Interactions that favor  $T = 1$  pairing lie below the diagonal. The only point above the diagonal corresponds to the  $(p_{1/2})^2 - (p_{1/2})^2$  matrix element. The pairing matrix elements and the symbols used are the same as in Figs. 2 and 13.

urations discussed in Sect. IV A. As a result, although the spin-triplet S-wave interaction is attractive, pairing matrix elements connecting different spin-orbit configurations,  $(j_{a>})^2 - (j_{b<})^2$  and  $(j_{a<})^2 - (j_{b>})^2$ , are repulsive. This can be seen clearly in the  $(d, d)$ ,  $(p, p)$ ,  $(f, f)$  and  $(p, f)$  groups at the  $^3S_1 - ^3D_1$  level in Figs. 12 and 13.

The next partial-wave contribution is due to the repulsive  $^1P_1$  spin-singlet channel (in contrast to the spin-triplet  $^3P_1$  for  $T = 1$  pairing), so that it decreases the attractive pairing strength of all  $T = 0, J = 1$  pairing matrix elements. Finally, Figs. 12 and 13 show smaller contributions due to the spin-triplet D waves, again with alternating attractive and repulsive character.

We compare the pairing strengths in the  $pf$  shell by plotting the  $T = 1, J = 0$  versus  $T = 0, J = 1$  pairing matrix elements in Fig. 14. This clearly demonstrates that nuclear forces in the  $pf$  shell favor  $T = 1$  over  $T = 0$  pairing, except for the  $(p_{1/2})^2 - (p_{1/2})^2$  matrix elements. This is in contrast with the expectation based on the relative S-wave interactions in free space, which favor the  $T = 0$  over  $T = 1$  channel, with a bound deuteron compared to the nearly-bound state in the  $^1S_0$  channel.

### A. Spin-orbit suppression

In addition to the effects of the repulsive  $^1P_1$  channel and of D waves, the suppression of  $T = 0$  pairing at the S-wave level in Fig. 14 is due to spin-orbit splitting between single-particle states. The impact of spin-orbit splitting on  $T = 0$  pairing properties has also been pointed out in shell-model calculations using empirical interactions [35, 36]. In our analysis, the significance of spin-orbit splitting lies in the choice of the  $jj$ -coupled ba-

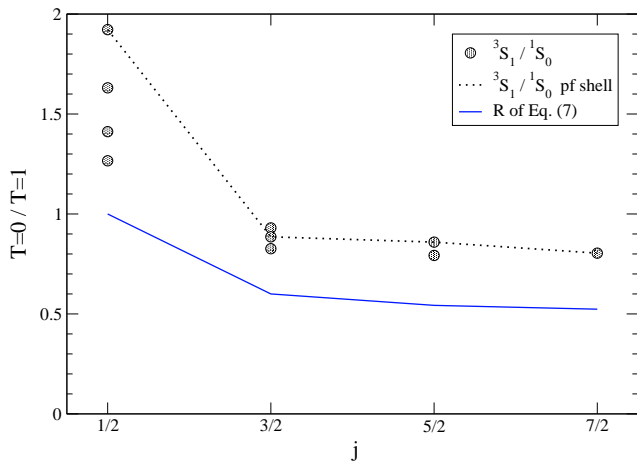


FIG. 15: Ratio of the diagonal  $(l_{aj_a})^2 - (l_{aj_a})^2$  pairing matrix elements in the  $T = 0, J = 1$  over the  $T = 1, J = 0$  channel. Results are shown including only S waves as a function of the total angular momentum  $j$  up to the  $pf$  shell. The dotted line connects the  $pf$ -shell matrix elements. The solid line is the ratio  $R$  of Eq. (7) for S-wave contact interactions with identical strengths.

sis and in our assumption that pairing matrix elements based on low-momentum interactions provide a first approximation for pairing in a  $j$ -shell [15, 16].

We discuss this first at the level of the  $^1S_0$  and  $^3S_1$  partial waves. The corresponding phase shifts [30] (and also low-momentum interactions [9, 10]) have very similar momentum dependences, because at low energies nuclear forces mainly differ by providing slightly more attraction in the  $T = 0$  channel to lead to a loosely bound deuteron. The similarity of the  $^1S_0$  and  $^3S_1$  channels is also reflected in large scattering lengths,  $a_{1S_0} = -23.768$  fm and  $a_{3S_1} = 5.420$  fm. At low energies, nuclear interactions are therefore close to Wigner's SU(4) limit, where S-wave contact interactions have identical strengths [37].

In order to study the ratio  $R$  of the  $T = 0, J = 1$  over the  $T = 1, J = 0$  pairing strengths, we consider two S-wave contact interactions with the same  $T = 1$  and  $T = 0$  strengths. The resulting pairing matrix elements can be calculated analytically (see, for example, Ref. [38]) and the ratio  $R$  is given by a geometrical factor:

$$\begin{aligned}
 R &= \frac{\langle n_a l j n_a l j | (1 - P_{12}) V_{3S_1} | n_b l j n_b l j \rangle_{J=1, T=0}}{\langle n_a l j n_a l j | (1 - P_{12}) V_{1S_0} | n_b l j n_b l j \rangle_{J=0, T=1}}, \\
 &= \frac{\begin{pmatrix} j & j & 1 \\ 1/2 & -1/2 & 0 \end{pmatrix}^2 + \begin{pmatrix} j & j & 1 \\ 1/2 & 1/2 & -1 \end{pmatrix}^2}{\begin{pmatrix} j & j & 0 \\ 1/2 & -1/2 & 0 \end{pmatrix}^2}, \\
 &= \frac{4j^2 + 4j + 3}{8j(j+1)}, \tag{7}
 \end{aligned}$$

where (...) are 3j symbols [28]. We find  $R = 1$  for  $j = 1/2$ ,  $R = 1/2$  in the limit of large  $j$ , and already  $R \leq 3/5$

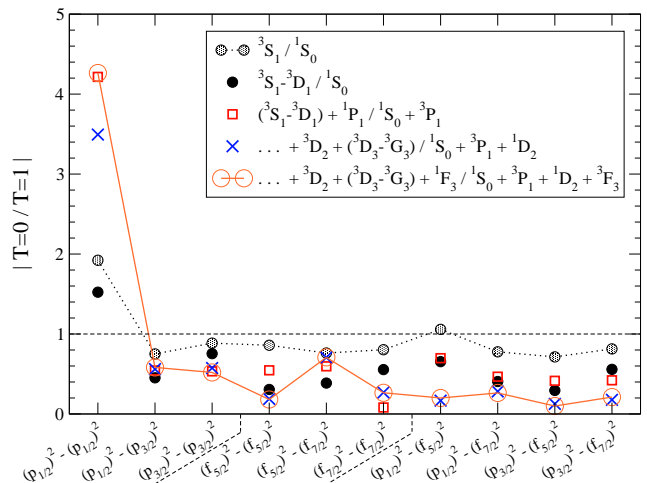


FIG. 16: Absolute value of the ratio of  $T = 0, J = 1$  over the  $T = 1, J = 0$  pairing matrix elements (all  $(l_{aj_a})^2 - (l_{bj_b})^2$ ) in the  $pf$  shell. The anomalously large ratio for the  $(p_{1/2})^2 - (p_{1/2})^2$  matrix element beyond S waves is due to the small  $T = 1, J = 0$  pairing matrix element in this case (see Fig. 2).

for  $j \geq 3/2$  [39]. This geometrical factor is due to the spin-orbit suppression and provides a simple explanation why S-wave nuclear forces favor  $T = 1, J = 0$  over  $T = 0, J = 1$  pairs, except in  $j = 1/2$  orbitals.

In Fig. 15, we compare the ratio  $R$  to the diagonal  $(l_{aj_a})^2 - (l_{aj_a})^2$  pairing matrix elements up to the  $pf$  shell. We find that the trend of Eq. (7) agrees nicely. As expected, the ratio is somewhat larger for low-momentum interactions, because the  $^3S_1$  part is more attractive than the  $^1S_0$  partial wave. For all  $j \geq 3/2$ , the  $T = 1, J = 0$  channel is favored. Finally, we include all partial-wave contributions and show in Fig. 16 the absolute value of the ratio of  $T = 0, J = 1$  over the  $T = 1, J = 0$  pairing matrix elements in the  $pf$  shell. This demonstrates that nuclear forces favor  $T = 1, J = 0$  over  $T = 0, J = 1$  pairing, except in low- $j$  orbitals.

The suppression  $R = 1/2$  in the limit of large  $j$  can be interpreted as a distribution of the  $^3S_1$  strength on more configurations, compared to the  $^1S_0$  case, because there are only two states for  $J = 0$ :  $(j_>) ^2$  and  $(j_<) ^2$ ; compared to four states for  $J = 1$ :  $(j_>) ^2$ ,  $(j_<) ^2$ ,  $(j_> j_<)$  and  $(j_< j_>)$ . In addition, a semiclassical picture for the suppression of  $T = 0$  pairing has been developed in Ref. [40].

## VII. CONCLUSIONS AND OUTLOOK

We have studied in detail partial-wave contributions of nuclear forces to pairing in nuclei, at the level of the pairing matrix elements and for neutron-neutron pairing gaps in semi-magic isotopic chains. For  $T = 1, J = 0$  pairing, the repulsive  $^3P_1$  channel decreases the LCS gaps by up to 15% compared to the gaps obtained from the standard  $^1S_0$  contribution, while the changes in the av-



erage gap were found to be small. The latter is due to the alternation of repulsive and attractive contributions for spin-triplet nuclear forces between paired nucleons. While we have focused on neutron-neutron pairing gaps, our conclusions equally apply to proton-proton gaps.

We expect the  ${}^3P_1$  effects will be more important for phenomena involving state-dependent pairing gaps, such as particle-transfer reactions. From the differences between the LCS and average gaps beyond the  ${}^1S_0$  channel, we conclude that future studies should compare directly calculated odd-even mass differences to the experimental gaps (see also Ref. [17]). Finally, important future work for pairing gaps is to include the effects of three-nucleon forces (for the impact in neutron matter, see Ref. [14]), many-body contributions or induced interactions [19, 20], and center-of-mass corrections to pairing interactions [26].

Based on the comparison of pairing matrix elements, we have shown that nuclear forces favor  $T = 1, J = 0$  over  $T = 0, J = 1$  pairing, except in low- $j$  orbitals. This is in contrast to the relative S-wave strengths in free space. We have traced the suppression of  $T = 0$  pairing to two origins. First is the spin-orbit splitting, which results in the  ${}^3S_1$  strength being distributed on more configurations, compared to the  ${}^1S_0$  strength in the case of  $T = 1$  pairing. In the SU(4) limit where both relative S-wave interactions are equally attractive, this leads to a relative

suppression of the pairing interaction for large- $j$  orbitals by a factor 1/2, in favor of the  $T = 1, J = 0$  case. The deuteron  ${}^3S_1$  channel would have to be twice as attractive as  ${}^1S_0$  to overcome this spin-orbit suppression. Second,  $T = 0$  pairing is weakened by the additional repulsive  ${}^1P_1$  channel and by the effects of D waves, more strongly compared to the effects of higher partial waves in the  $T = 1$  pairing case. Our findings render the standard free-space motivation for  $T = 0$  pairing at best incomplete.

## Acknowledgments

We are grateful to G. F. Bertsch for discussions on  $T = 0$  pairing and also thank T. Duguet, K. Hebeler, V. Koch, T. Lesinski and A. Pastore for useful conversations. This work was supported in part by the UNEDF SciDAC Collaboration under DOE Grant DE-FC02-07ER41457, the NSF under Grant 0835543, the DOE under Contract No. DE-AC02-05CH11231 (LBNL), the Natural Sciences and Engineering Research Council of Canada (NSERC) and the Helmholtz Alliance Program of the Helmholtz Association, contract HA216/EMMI “Extremes of Density and Temperature: Cosmic Matter in the Laboratory”. TRIUMF receives funding via a contribution through the National Research Council Canada.

- 
- [1] M. Bender, P.-H. Heenen and P.-G. Reinhard, *Rev. Mod. Phys.* **75**, 121 (2003).
  - [2] G. F. Bertsch, B. Sabbey and M. Uusnäkki, *Phys. Rev. C* **71**, 054311 (2005).
  - [3] M. Kortelainen, J. Dobaczewski, K. Mizuyama and J. Toivanen, *Phys. Rev. C* **77**, 064307 (2008).
  - [4] J. E. Drut, R. J. Furnstahl and L. Platter, *Prog. Part. Nucl. Phys.* **64**, 120 (2010).
  - [5] N. Kaiser, S. Fritsch and W. Weise, *Nucl. Phys. A* **724**, 47 (2003).
  - [6] S. K. Bogner, R. J. Furnstahl and L. Platter, *Eur. Phys. J. A* **39**, 219 (2009).
  - [7] M. Stoitsov, J. Moré, W. Nazarewicz, J. C. Pei, J. Sarich, N. Schunck, A. Staszczak and S. Wild, *J. of Physics: Conf. Series* **180**, 012082 (2009).
  - [8] B. Gebremariam, T. Duguet and S. K. Bogner, arXiv:0910.4979 [nucl-th].
  - [9] S. K. Bogner, T. T. S. Kuo and A. Schwenk, *Phys. Rept.* **386**, 1 (2003).
  - [10] S. K. Bogner, R. J. Furnstahl, S. Ramanan and A. Schwenk, *Nucl. Phys. A* **784**, 79 (2007).
  - [11] S. K. Bogner, R. J. Furnstahl and R. J. Perry, *Phys. Rev. C* **75**, 061001(R) (2007).
  - [12] S. K. Bogner, A. Schwenk, R. J. Furnstahl and A. Nogga, *Nucl. Phys. A* **763**, 59 (2005).
  - [13] S. K. Bogner, R. J. Furnstahl, A. Nogga and A. Schwenk, arXiv:0903.3366 [nucl-th].
  - [14] K. Hebeler and A. Schwenk, arXiv:0911.0483 [nucl-th].
  - [15] T. Duguet and T. Lesinski, *Eur. Phys. J. ST* **156**, 207 (2008).
  - [16] T. Lesinski, T. Duguet, K. Bennaceur and J. Meyer, *Eur. Phys. J. A* **40**, 121 (2009).
  - [17] T. Duguet and T. Lesinski, *AIP Conf. Proc.* **1165**, 243 (2009).
  - [18] K. Hebeler, T. Duguet, T. Lesinski and A. Schwenk, *Phys. Rev. C* **80**, 044321 (2009).
  - [19] F. Barranco, R. A. Broglia, G. Colò, G. Gori, E. Vigezzi and P. F. Bortignon, *Eur. Phys. J. A* **21**, 57 (2004).
  - [20] A. Pastore, F. Barranco, R. A. Broglia and E. Vigezzi, *Phys. Rev. C* **78**, 024315 (2008).
  - [21] K. Hebeler, A. Schwenk and B. Friman, *Phys. Lett. B* **648**, 176 (2007).
  - [22] See, for example, W. Satula, *Phys. Scr.* **T125**, 82 (2006) or A. L. Goodman, *Adv. Nucl. Phys.* **11**, 263 (1979).
  - [23] P. Ring and P. Schuck, *The Nuclear Many-Body Problem* (Springer, New York, 1980).
  - [24] E. Chabanat, P. Bonche, P. Haensel, J. Meyer and R. Schaeffer, *Nucl. Phys. A* **635**, 231 (1998).
  - [25] D. R. Entem and R. Machleidt, *Phys. Rev. C* **68**, 041001(R) (2003).
  - [26] H. Hergert and R. Roth, *Phys. Rev. C* **80**, 024312 (2009).
  - [27] A. Bohr and B. R. Mottelson, *Nuclear Structure* (World Scientific Publishing Company, 1998), Vol. 1.
  - [28] D. A. Varshalovich, A. N. Moskalev, and V. K. Khersonskii, *Quantum Theory of Angular Momentum* (World Scientific, 1988).
  - [29] We use the Talmi-Moshinsky brackets as in G. P. Kamuntavičius, R. K. Kalinauskas, B. R. Barrett, S. Mickevičius and D. Germanas, *Nucl. Phys. A* **695**, 191 (2001).
  - [30] V. G. J. Stoks, R. A. M. Klomp, M. C. M. Rentmeester

- and J. J. de Swart, Phys. Rev. C **48**, 792 (1993); and <http://nn-online.org>.
- [31] D. M. Brink and R. A. Broglia, *Nuclear Superfluidity: Pairing in Finite Systems* (Cambridge University Press, Cambridge, 2005).
- [32] W. Satula, J. Dobaczewski and W. Nazarewicz, Phys. Rev. Lett. **81**, 3599 (1998).
- [33] T. Duguet, P. Bonche, P.-H. Heenen and J. Meyer, Phys. Rev. C **65**, 014311 (2001).
- [34] G. Audi, A. H. Wapstra and C. Thibault, Nucl. Phys. A **729**, 337 (2003).
- [35] A. Poves and G. Martinez-Pinedo, Phys. Lett. B **430**, 203 (1998).
- [36] G. Martinez-Pinedo, K. Langanke and P. Vogel, Nucl. Phys. A **651**, 379 (1999).
- [37] T. Mehen, I. W. Stewart and M. B. Wise, Phys. Rev. Lett. **83**, 931 (1999).
- [38] K. L. G. Heyde, *The Nuclear Shell Model* (Springer, Berlin, 1994).
- [39] G. F. Bertsch, A. O. Macchiavelli and A. Schwenk, unpublished; A. Schwenk, talk given at UNEDF Annual Meeting, Pack Forest, WA, 2007.
- [40] G. F. Bertsch and S. Baroni, arXiv:0904.2017v2 [nucl-th].